

Solid-angle based nearest-neighbor algorithm adapted for systems with low coordination number

A. Ulugöl,¹ F. Smallenburg,² and L. Filion¹

¹*Soft Condensed Matter and Biophysics Group, Debye Institute for Nanomaterials Science, Utrecht University, Princetonplein 1, Utrecht, 3584 CC, Netherlands*

²*Laboratoire de Physique des Solides, Université Paris-Saclay, Orsay, 91405, France*

(*Electronic mail: a.ulugol@uu.nl.)

(Dated: 17 November 2025)

Nearest-neighbor identification is central to the analysis of local structure in condensed matter systems. The solid-angle-based nearest-neighbor (SANN) algorithm is widely used offering a parameter-free and computationally efficient alternative to cutoff- or Voronoi-based methods. Unfortunately, however, in systems with low coordination numbers, SANN tends to identify many particles as neighbors that are outside the nearest neighbor shell. Here, we propose a solution to this problem. Specifically, we propose a geometric modification, the “inscribed circle modification”, that resolves systematic overcounting in low-coordination lattices without introducing free parameters. We benchmark the modified algorithm (mSANN) against Voronoi and the original SANN algorithm in crystalline, quasicrystalline, and heterogeneous systems, and demonstrate that it provides robust and low-cost neighbor identification across both two and three dimensions.

I. INTRODUCTION

Identifying nearest neighbors (NNs) is central to the analysis of local structure in many-body systems, and underlies a wide range of order parameters and classification methods.^{1–5} Despite its prevalence, no unique definition of NNs exists, and several algorithms are routinely employed.

The most direct approach is to impose a fixed-distance cutoff. A typical choice is the first minimum of the pair correlation function $g(r)$, which captures the first coordination shell. While effective in homogeneous systems, this definition becomes ambiguous in the presence of density gradients or phase coexistence, where a single cutoff cannot account for spatial variations.

An alternative is the Voronoi construction, which partitions space into polyhedra that tessellate the system.⁶ Two particles are defined as neighbors if their Voronoi cells share a face in 3D or edge in 2D. This approach is geometrical and parameter-free, and is often applied to inhomogeneous systems. However, it suffers from two drawbacks: sensitivity to thermal fluctuations, which leads to fluctuations in the number of neighbors even in a stable lattice, and systematic overcounting in low-coordination structures. Several weighted variants have been proposed,^{3,7–9} but these introduce additional parameters. Moreover, Voronoi tessellations are computationally demanding in three dimensions, which limits their use in on-the-fly analyses.

In 2012, van Meel *et al.* introduced the solid-angle-based nearest-neighbor (SANN) algorithm as a parameter-free and computationally inexpensive alternative.¹⁰ SANN assigns a solid angle to each candidate neighbor and defines the cutoff radius such that the sum of solid angles completes a sphere. This construction satisfies four desirable criteria: (i) absence of free parameters, (ii) robustness to thermal noise, (iii) low computational cost, and (iv) applicability to inhomogeneous systems. Nevertheless, the method has two limitations. First, a direct extension, such as presented in Ref. 11, is less efficient in two dimensions as solving for the cutoff radius re-

quires a numerical root-finding step. A solution to this issue was presented in Ref. 12, where they reformulate the problem as an existence-uniqueness problem (which they call SAN-Nex). Second, like Voronoi, it overestimates neighbor counts in low-coordination lattices (e.g. honeycomb or diamond). The original work¹⁰ suggested introducing a tuning parameter to address the latter, at the expense of losing strict parameter-free character. Other extensions to SANN include an effort to take into consideration anisotropy in the environment¹³ and a variation aimed at making it more applicable for polydisperse systems (SANNR)¹⁴.

In this paper, we revisit the foundations of SANN and examine in detail two modifications. First, following Ref. 12 we reformulate the cutoff condition to enable an efficient two-dimensional implementation, and then look in detail at this change. Second, we introduce a simple geometric modification, the “inscribed circle (sphere) trick”, that eliminates systematic overcounting in low-coordination lattices without introducing free parameters. We compare the modified SANN (mSANN) with Voronoi and the original SANN across crystalline, quasicrystalline, and coexistence systems in both two and three dimensions, and show that it provides robust and efficient neighbor identification across a broad range of environments.

II. METHOD DESCRIPTION AND RESULTS

We begin by revisiting the original formulation of the solid-angle-based nearest-neighbor (SANN) algorithm¹⁰ and then present its extension to two dimensions^{11,12}. The discussion proceeds in three steps: (i) the three-dimensional definition, (ii) its extension to two dimensions, and (iii) a new variation (mSANN) that addresses overcounting of distant neighbors.

A. Description and Extension of SANN

The fixed-distance cutoff method defines neighbors of particle i as those j with $|\mathbf{r}_{ij}| < R$, where R is a global parameter. While straightforward, this definition requires system-dependent tuning. SANN eliminates this parameter by assigning each particle i a local cutoff R_i , determined such that the angular space around i is exactly filled by its neighbors.

For a trial cutoff R_i , each candidate neighbor j spans a solid angle θ_{ij} . SANN defines R_i by requiring that the sum of these angles completes the full surrounding sphere: 4π in three dimensions, 2π in two. In practice, only the distances $r_{ij} = |\mathbf{r}_{ij}|$ of the closest neighbors need to be considered.

In three dimensions the m -neighbor shell radius $R_i^{(m)}$ is obtained from the linear relation

$$4\pi = \sum_{j=1}^m 2\pi \left(1 - \frac{r_{ij}}{R_i^{(m)}} \right), \quad (1)$$

which can be solved directly for $R_i^{(m)}$.

In two dimensions, replacing the sphere by a circle yields the nonlinear condition

$$\pi = \sum_{j=1}^m \theta_{ij} = \sum_{j=1}^m \arccos \left(\frac{r_{ij}}{R_i^{(m)}} \right), \quad (2)$$

where θ_{ij} is half the central angle of the chord associated with neighbor j as shown in Fig. 1. Unlike Eq. (1), Eq. (2) cannot be solved in closed form. It can be solved via a root-finding algorithm, at extra numerical cost.

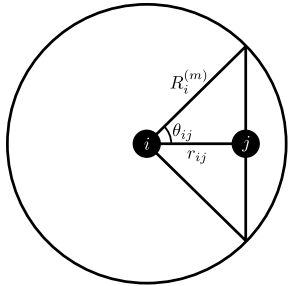


FIG. 1: Angle θ_{ij} associated with the chord passing through neighbor j . $R_i^{(m)}$ denotes the shell radius of particle i with m neighbors, and r_{ij} is the distance between i and j .

To retain the efficiency of SANN in two dimensions, as shown in Ref. 12, the problem can be cast in terms of existence rather than an explicit solution. Define

$$f_i(x; m) = -\pi + \sum_{j=1}^m \arccos \left(\frac{r_{ij}}{x} \right), \quad x \geq r_{im}. \quad (3)$$

Note that $f_i(R_i^{(m)}; m) = 0$ by construction. Since \arccos is strictly decreasing, $f_i(x; m)$ is strictly increasing in x and thus admits a unique root. It follows that $R_i^{(m)}$ lies within the interval $[r_{im}, r_{i,m+1})$ if and only if

$$f_i(r_{i,m+1}; m) > 0 \quad \text{and} \quad f_i(r_{i,m}; m-1) < 0. \quad (4)$$

This observation leads to a simple iterative procedure: starting from $m = 3$ (the minimum possible SANN coordination in two dimensions), increment m until the above condition is satisfied. The corresponding m then defines the coordination number of particle i , and the neighbor set is $\mathcal{N}_b(i) = \{j\}_{j=1}^m$. Unlike the original formulation, this approach generalizes directly to arbitrary dimension while avoiding nonlinear root finding.

B. Algorithm

A step-by-step procedure (analogous to Ref. 12) to identify the nearest neighbors of particle i as we have introduced in subsection II A is given by:

1. Compute distances r_{ij} to all potential neighbors $\{j\}$ from particle i .
2. Sort possible neighbors $\{j\}$ by their distance r_{ij} in increasing order such that $r_{ij} \leq r_{i,j+1}$.
3. Set $m = 3$ (i.e., the minimum number of neighbors).
4. Compute $f_i(r_{i,m+1}; m)$.
5. if $f_i(r_{i,m+1}; m) \leq 0$ then increment m by 1 and go back to step 4.
6. Otherwise, m is the number of neighbors for particle i , and $\mathcal{N}_b(i) = \{j\}_{j=1}^m$ is the associated set of neighbors.

C. Algorithm Properties

The two-dimensional extension of SANN retains several properties of the original three-dimensional algorithm, while introducing a few modifications. In what follows we examine six key aspects:

1. **Convergence:** the iterative procedure always terminates provided that a sufficient number of candidate neighbors exist.
2. **Equidistant neighbors:** if multiple particles are equidistant from a given particle, then either all or none are identified as neighbors.
3. **Pairwise symmetry:** neighbor relations need not be symmetric, though simple symmetrization schemes can be applied when required.
4. **Tiling generation:** in two dimensions, neighbor relations can be used to construct a consistent tiling of the plane.
5. **Local area estimation:** the algorithm provides an approximate measure of the area associated with each particle.
6. **Higher-order neighbors:** the identification can be iterated to obtain next-nearest neighbors and beyond.

Properties (iii) and (vi) are unchanged from the original three-dimensional formulation¹⁰. Properties (i), (ii), and (v) require modified arguments in two dimensions, and property (iv) is specific to the two-dimensional extension introduced here.

1. Convergence

Lemma. The iterative procedure defining $R_i^{(m)}$ converges, provided a sufficient number of candidate neighbors exist.

Proof. Let $R_i^{(m)}$ and $R_i^{(m+1)}$ denote the shell radii obtained when m and $m+1$ neighbors are included. By definition,

$$f_i(R_i^{(m)}; m) = 0, \quad f_i(R_i^{(m+1)}; m+1) = 0,$$

where $f_i(x; m) = -\pi + \sum_{j=1}^m \arccos(r_{ij}/x)$. Taking the difference gives

$$\begin{aligned} 0 &= f_i(R_i^{(m+1)}; m+1) - f_i(R_i^{(m)}; m) \\ &= \arccos\left(\frac{r_{i,m+1}}{R_i^{(m+1)}}\right) \\ &\quad + \sum_{j=1}^m \left[\arccos\left(\frac{r_{ij}}{R_i^{(m+1)}}\right) - \arccos\left(\frac{r_{ij}}{R_i^{(m)}}\right) \right]. \end{aligned} \quad (5)$$

The first term is positive since $r_{i,m+1} < R_i^{(m+1)}$. Hence the sum in Eq. (5) must be negative:

$$\sum_{j=1}^m \left[\arccos\left(\frac{r_{ij}}{R_i^{(m+1)}}\right) - \arccos\left(\frac{r_{ij}}{R_i^{(m)}}\right) \right] < 0.$$

Because $\arccos(x)$ is strictly decreasing, each term satisfies

$$\arccos\left(\frac{r_{ij}}{R_i^{(m+1)}}\right) < \arccos\left(\frac{r_{ij}}{R_i^{(m)}}\right),$$

implying

$$R_i^{(m+1)} < R_i^{(m)}.$$

Thus, the cutoff radius decreases monotonically with m , ensuring convergence.

2. Equidistant neighbors

Lemma. If two or more particles are equidistant from particle i , then either all or none of them are identified as neighbors.

Proof. Suppose, for contradiction, that two particles satisfy $r_{im} = r_{i,m+1}$, yet only one is included, so that the algorithm converges with $\mathcal{N}_b(i) = m$. This requires $f_i(r_{i,m+1}; m) > 0$. Since $r_{im} = r_{i,m+1}$, it follows that $f_i(r_{im}; m) > 0$ as well.

Now observe that

$$\begin{aligned} f_i(r_{im}; m) &= -\pi + \sum_{j=1}^m \arccos\left(\frac{r_{ij}}{r_{im}}\right) \\ &= -\pi + \sum_{j=1}^{m-1} \arccos\left(\frac{r_{ij}}{r_{im}}\right) \\ &= f_i(r_{im}; m-1). \end{aligned} \quad (6)$$

Hence $f_i(r_{im}; m-1) > 0$, which would force the algorithm to converge with $\mathcal{N}_b(i) = m-1$. This contradicts the assumption that exactly one of the equidistant neighbors was included.

Therefore, the algorithm cannot separate equidistant particles: they are either all included or all excluded.

3. Pairwise symmetry

Property. SANN does not guarantee pairwise symmetry: if particle j is identified as a neighbor of i , the converse need not hold.

Explanation. This asymmetry arises because SANN assigns a distinct cutoff radius R_i to each particle. Thus j may lie within R_i while i lies outside R_j . Such cases are rare and typically occur only in systems with strong density gradients. For most applications, this lack of symmetry does not affect neighbor-dependent observables.

Symmetrisation strategies. When pairwise symmetry is required, two post-processing options are available, as proposed by the original work¹⁰:

- *Additive symmetrisation:* if (i, j) is asymmetric, add the missing link so that i and j become mutual neighbors.
- *Subtractive symmetrisation:* if (i, j) is asymmetric, remove the link entirely so that neither particle lists the other as neighbor.

The choice between these schemes is application-dependent, as neither is inherently preferable.

4. Tiling generation

In two-dimensional systems it is often desirable to construct a tiling representation of the particle network, for example when analyzing quasicrystalline order. The 2D extension of SANN provides a natural basis for such a construction.

Procedure. A tiling can be generated in four steps:

1. Identify the nearest neighbors of all particles using SANN.
2. Apply a symmetrisation scheme (Sec. II C 3) to ensure pairwise consistency.
3. Connect each pair of neighboring particles with a line segment.
4. If two line segments intersect, remove the longer one.

The resulting network defines a tiling in which each particle corresponds to a vertex. This approach is straightforward to implement and yields tessellations consistent with the local connectivity identified by SANN.

5. Local area

Estimating local particle areas can be useful, for instance when analyzing phase coexistence. Voronoi tessellation remains the natural choice for such tasks, since it provides exact local cells. Nevertheless, SANN can serve as a lightweight alternative.

In three dimensions, the cutoff radius R_i follows directly from the SANN condition and defines a sphere of radius R_i , yielding the local volume¹⁰. In two dimensions, our extension only determines the interval in which R_i must lie. From this point, two options are available: (i) solve for R_i explicitly using a root-finding procedure, or (ii) approximate R_i by the midpoint of the interval. The local area is then assigned as the disk of radius R_i .

While less accurate than Voronoi tessellation, this approach offers a computationally inexpensive estimate of local densities, sufficient for many structural analyses.

Note that more detailed and complex analysis of local free volumes starting from SANN is also possible, see Ref. 12.

6. Next-nearest neighbors

The identification of next-nearest neighbors carries over directly from the original three-dimensional SANN¹⁰. The procedure is iterative: (i) determine the nearest neighbors of a particle using the algorithm in Sec. II B; (ii) remove these neighbors from the candidate set; (iii) rerun the algorithm beginning from step 3.

The new set of neighbors corresponds to the next-nearest neighbors of the particle. Repeating this procedure allows identification of the n^{th} neighbor shell in a consistent manner.

D. Geometric modification based on the inscribed circle/sphere (mSANN)

Up to this point, we have emphasized the advantages of parameter-free neighbor definitions such as SANN and Voronoi over fixed-distance cutoffs. However, both SANN and Voronoi systematically overcount neighbors in lattices with low coordination number (CN)¹⁰. Here, we define “overcounting” as the identification of particles that lie beyond the first minimum of the radial distribution function as neighbors – in the absence of density gradients. As we will see later in this paper, this includes e.g. the honeycomb (CN=3) and square (CN=4) lattices in two dimensions, and the α -graphite (CN=3), diamond (CN=4), simple cubic (CN=6), and body-centered cubic (CN=8) lattices in three dimensions. While in principle there is no “correct” definition of nearest neighbors,

this often leads to the inclusion of neighbors that one would not intuitively consider to be part of the first neighbor shell.

For Voronoi-based algorithms, a common remedy for this issue is to weight neighbors by the area (or length) of their shared boundary,^{3,7-9} but this introduces additional parameters. For SANN, van Meel *et al.*¹⁰ proposed modifying Eq. (1) by multiplying 4π with a free parameter. While this alleviates overcounting, it breaks the strict parameter-free character of the algorithm. Here we propose an alternative, parameter-free correction based on the underlying geometry.

Geometric interpretation in 2D

Consider a particle i with m neighbors according to SANN. Around i , draw a circle of radius R_i and for each neighbor, draw a chord such that the neighbor lies at the midpoint of that chord. The set of these chords, when rearranged, defines a cyclic m -gon. (Fig. 2). Equation (2) then guarantees that this polygon is circumscribed around the circle of radius R_i . Importantly, SANN depends only on neighbor distances, not directions, so a local rotation can always map the configuration to such a cyclic polygon.

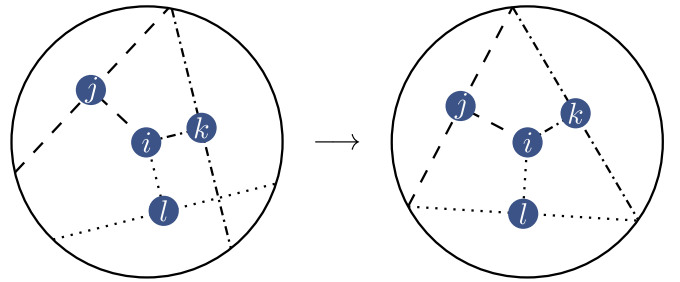


FIG. 2: Interpretation of Eq. (2) in two dimensions. Local rotations around particle i map neighbor positions onto the midpoints of a cyclic polygon, with R_i as the radius of the circumscribed circle.

Ideal lattices and overcounting

In the ideal case of m equidistant, equally spaced neighbors, the corresponding polygon is regular and the neighbors lie on its inscribed circle (Fig. 3). Standard SANN, however, uses the circumscribed circle. For low m , the ratio $r_{\text{in}}/r_{\text{cir}}$ is small, causing R_i to be overestimated. As a result, SANN may enclose not only the true nearest neighbors but also next-nearest neighbors.

For example, in a perfect honeycomb lattice ($m = 3$), the circumscribed circle of the associated triangle has radius $2a$ (a being the lattice constant), which includes both next- and next-next-nearest neighbors (Fig. 4). This prevents the algorithm from converging to the correct CN.

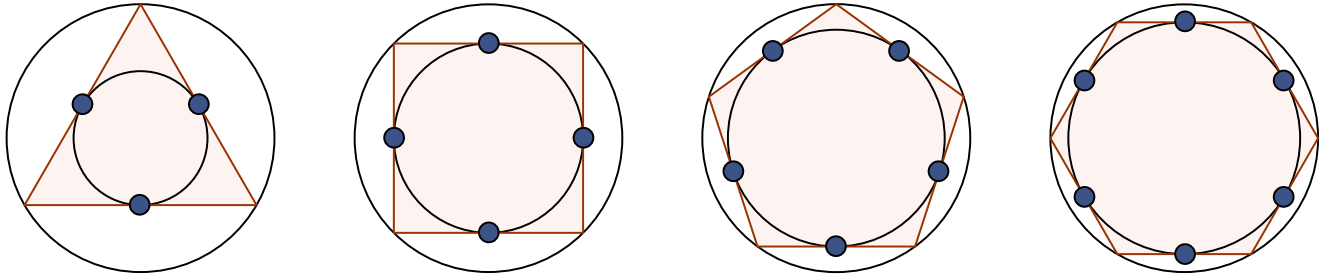


FIG. 3: Inscribed and circumscribed circles of the first four regular polygons.

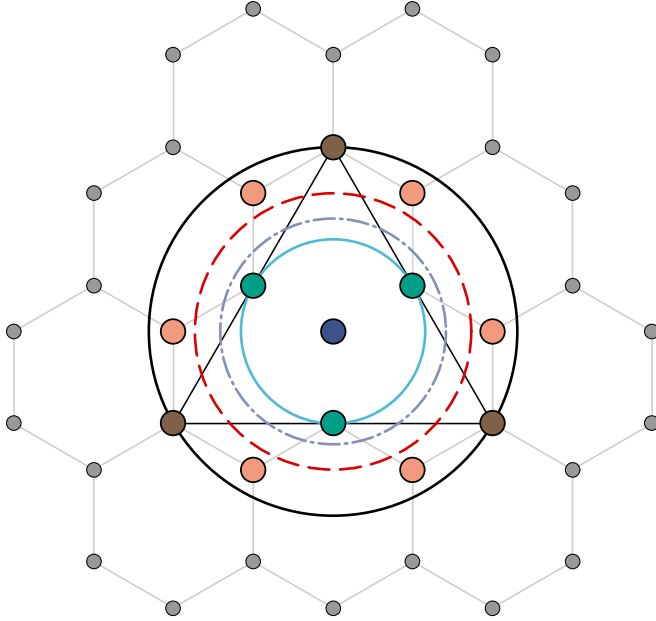


FIG. 4: SANN applied to an ideal honeycomb lattice. The outer circle (circumscribed) leads to overcounting, while the inscribed circle yields the correct CN. Arithmetic and geometric mean circles (dashed and dot-dashed) both eliminate overcounting.

The inscribed circle modification

For a regular m -gon, the ratio of inscribed to circumscribed radius is

$$\frac{r_{\text{in}}}{r_{\text{cir}}} = \cos\left(\frac{\pi}{m}\right). \quad (7)$$

We therefore propose replacing the circumscribed circle in SANN by an averaged circle between r_{in} and r_{cir} . Choosing the arithmetic mean, the modified convergence criterion becomes

$$\exists ! R_i \text{ s.t. } r_{im^*} \leq k_m R_i < r_{i,m^*+1} \iff f_i(r_{i,m^*+1}/k_m; m^*) > 0, \quad (8)$$

with

$$k_m = \frac{1}{2} [1 + \cos(\pi/m)]. \quad (9)$$

We refer to this parameter-free modification as the *inscribed circle trick*, and the variation including this trick as mSANN. In practice, both arithmetic and geometric means resolve the overcounting (Fig. 4), but the arithmetic mean preserves greater robustness to thermal fluctuations.

This modification, however, breaks the strict equidistant-neighbor property (Sec. II C 2); care must therefore be taken to verify robustness in cases with degeneracies.

Extension to 3D

An analogous argument applies in three dimensions. In this case the shell radius has a closed-form expression,

$$R_i = \frac{\sum_{j=1}^m r_{ij}}{m-2}. \quad (10)$$

For a perfect lattice, all neighbors are equidistant ($r_{ij} = r_{NN}$), which suggests modifying R_i by the geometric mean

$$R_i^{GM} = \sqrt{r_{NN} R_i} = R_i \sqrt{1 - \frac{2}{m}}. \quad (11)$$

E. Bulk phases

We first benchmark Voronoi, SANN, and mSANN in bulk crystalline systems without density gradients. In two dimensions, we consider honeycomb, square, and hexagonal lattices, which have coordination numbers (CN) of 3, 4, and 6, respectively. The honeycomb and square lattices were generated from Monte Carlo simulations¹⁵ of binary mixtures of hard disks, retaining only the large species. Specifically, for the honeycomb lattice we used a system with a size ratio of 0.386 and a packing fraction of 0.797, where the holes between large particles were filled by seven small particles each. For the square lattice we used a size ratio of 0.45 and a packing fraction of 0.803, with each square hole between large particles containing one small particle. The hexagonal lattice was obtained from a Monte Carlo¹⁵ simulation of 512 Lennard-Jones disks in the canonical ensemble at density $\rho\sigma^2 = 0.9$ and interaction strength $\beta\varepsilon = 2$. In three dimensions, we analyze simple cubic (SC), body-centered

cubic (BCC), face-centered cubic (FCC), hexagonal close-packed (HCP), cubic diamond, and α -graphite. Ideal configurations with 1000–1372 particles were prepared and perturbed by uncorrelated Gaussian displacements of standard deviation $0.05a$, where a is the lattice constant.

Two dimensions. Representative neighbor networks are shown in Fig. 5, and the resulting CN distributions in Fig. 6. For honeycomb and square lattices, Voronoi strongly overestimates the CN (peak at 6), while SANN reduces but does not eliminate this bias (peak at 5). By contrast, mSANN identifies the correct CN for all particles, yielding a sharp distribution. In the hexagonal lattice, Voronoi and SANN both recover CN=6 for all particles, whereas mSANN assigns CN=5 to about 20% of the particles, arising from opposing thermal displacements of neighboring particles.

Three dimensions. For ideal lattices (Fig. 7), Voronoi and SANN coincide except for SC and α -graphite. In SC, Voronoi yields the correct CN while SANN overestimates. In α -graphite, Voronoi correctly identifies in-plane neighbors but also includes spurious interplane neighbors, while SANN includes both nearest and next-nearest neighbors. In contrast, mSANN recovers the correct CN for all six structures.

Adding Gaussian noise broadens the distributions (Fig. 8). For low-CN lattices (SC, BCC, cubic diamond, α -graphite), mSANN remains closest to the expected CN, confirming its correction of the overcounting problem. For high-CN lattices (FCC, HCP), SANN gives the most consistent results, indicating superior robustness under thermal fluctuations. Voronoi shows broad distributions in all but the BCC lattice, where it achieves its highest consistency.

Summary. Across bulk phases, mSANN consistently outperforms Voronoi and SANN for lattices with low coordination, while standard SANN remains preferable for highly coordinated structures subject to thermal fluctuations.

F. 12-fold symmetric quasicrystal approximants

To further test the algorithms in two dimensions, we consider phases with multiple coordination numbers, namely 12-fold symmetric quasicrystals (QC12). These structures consist of squares and triangles and naturally exhibit CNs of 4, 5, and 6, providing a benchmark for environments with fluctuating local density.

We analyze two realizations of the approximant: (i) a Stampfli tiling¹⁶ and (ii) a random square–triangle tiling of 1224 particles. The Stampfli configuration was generated as an ideal tiling, which was then decorated with a binary mixture of additive hard disks of size ratio 0.4, where the large disks sit at the vertices of the tiling, while the small disks sit at the centers of the squares. This configuration was then equilibrated at a packing fraction 0.824. The random square–triangle tiling was obtained by applying zipper moves¹⁷ to the Stampfli configuration, followed by the same equilibration protocol.

All three algorithms were applied to both realizations. Representative results are shown in Fig. 9, where identified square tiles are highlighted in orange for clarity, and the resulting CN

distributions are given in Fig. 10.

First, we observe that Voronoi construction fails to identify any square tiles, which is a consequence of its intrinsic triangulation. By design, it cannot generate non-triangular polygons without additional post-processing. This is reflected in Fig. 10, where Voronoi consistently yields an average CN of 6 for both approximants.

In contrast, both SANN and mSANN successfully recover square tiles. For the Stampfli tiling, the two algorithms give nearly identical results, including the distribution of CNs. Differences emerge in the randomized tilings, particularly in square-dominated regions: SANN often introduces spurious links across square diagonals, inflating the CN, whereas mSANN preserves the intended square topology.

These results highlight a key advantage of mSANN in complex environments. Unlike Voronoi, which is restricted to triangulations, and unlike SANN, which is prone to overcounting in low-CN motifs, mSANN consistently reproduces the intended local topology of quasicrystal approximants. This robustness across heterogeneous local environments suggests that mSANN is well suited for the analysis of disordered or aperiodic phases, where multiple coordination numbers coexist.

G. Coexisting phases and defects

As a final test case, we analyze two structures that include a phase coexistence: QC12–hexagonal and QC12–square. These systems combine multiple coordination numbers (4, 5, and 6) with interfaces and defects, providing a comprehensive benchmark for algorithm robustness.

Both coexistence states were generated by simulating square-shoulder particles in the canonical ensemble, with pair potential

$$V(r) = \begin{cases} \infty & r \leq \sigma, \\ \varepsilon & \sigma < r \leq \delta, \\ 0 & \delta < r, \end{cases} \quad (12)$$

where r is the interparticle distance, σ the particle diameter, ε the shoulder height, and $\delta = 1.4\sigma$ the shoulder width. The phase behavior of this system was studied extensively and it is known to form 12-fold QC, hexagonal and square lattices^{18–20}.

To generate the QC12–hexagonal coexistence, we start from a hexagonal lattice and replace its central region with a patch of the Stampfli tiling. Each vertex is then decorated with a square-shoulder particle with interaction strength $\varepsilon/k_B T = 3.333$, resulting in a total of $N = 1865$ particles at a number density of $\rho\sigma^2 = 1.032$. The configuration was subsequently equilibrated using event-driven molecular dynamics (EDMD)²¹.

The QC12–square coexistence was prepared analogously, starting from a square lattice. The resulting system contained $N = 1481$ particles at a number density of $\rho\sigma^2 = 0.9542$, and was likewise equilibrated using EDMD²¹.

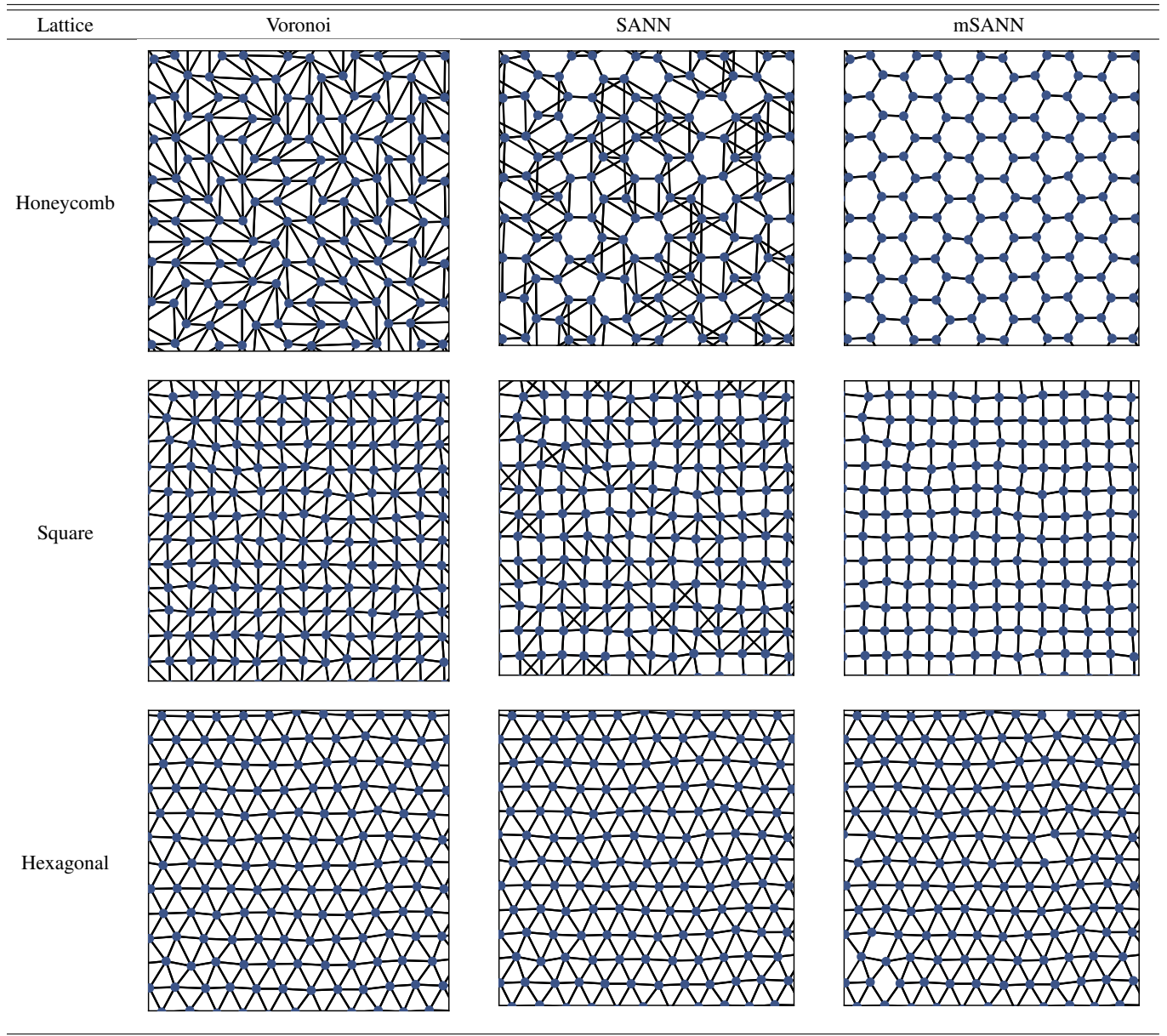


FIG. 5: Comparison of nearest-neighbor identification in 2D lattices using Voronoi, SANN, and mSANN. Dots represent particles and line segments connect the neighbors. Configurations include correlated thermal noise.

The Voronoi construction again fails to capture non-triangular tiles, so the comparison focuses on SANN and mSANN. In the QC12–hexagonal coexistence, both variants correctly recover squares, triangles, and pentagons (the latter corresponding to defects). SANN, however, undercounts in square-rich regions, often connecting diagonals across squares and thereby reducing the apparent number of squares. By contrast, mSANN captures both the missing squares and most pentagons, though it occasionally merges adjacent triangles into quadrilaterals in hexagonal domains.

The QC12–square coexistence shows similar behaviour. Here mSANN more reliably identifies the defects, including two shapes of defects corresponding to irregular hexagons²²,

which SANN misses in the majority of cases. Voronoi remains highly effective in pure hexagonal domains but offers no advantage in the mixed regions.

Overall, these tests confirm the complementary strengths of the algorithms. Voronoi is best suited to purely hexagonal environments but cannot describe non-triangular tiles. SANN and mSANN are both capable of analyzing coexisting phases, with mSANN providing more consistent identification in low-CN regions and superior detection of defect structures.

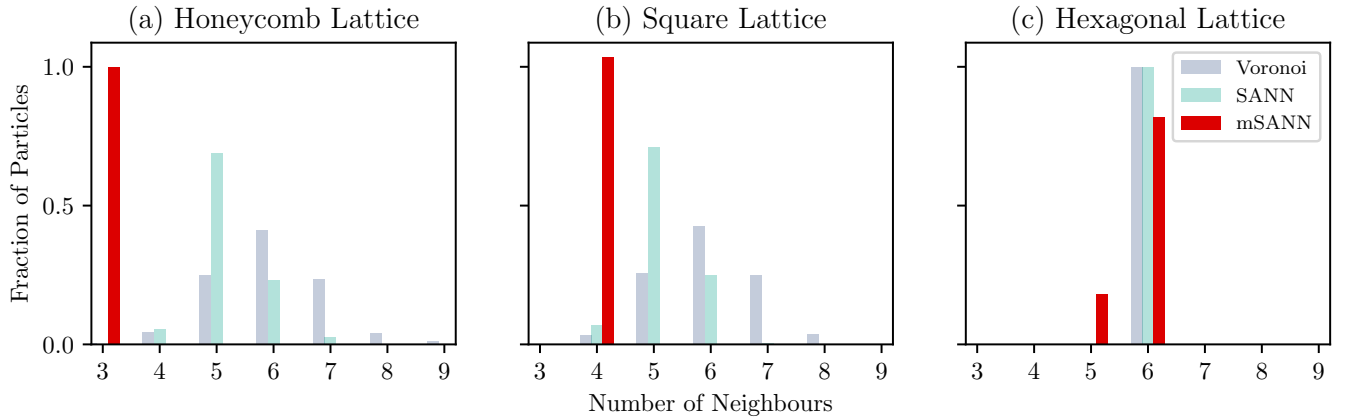


FIG. 6: Distributions of coordination numbers in 2D lattices identified using Voronoi, SANN, and mSANN: (a) honeycomb, (b) square, (c) hexagonal lattices corresponding to those shown in Fig. 5.

H. Performance analysis

Low computational cost is a key requirement for a “good” neighbor-identification algorithm. To assess this property, we implemented the two-dimensional extension of SANN in Python and optimised it for speed. The computational bottlenecks are pair-distance evaluation and sorting, which scale as $\mathcal{O}(N^2)$ in naive implementations. To reduce this cost, we employ a k -d tree, which combines proximity search and sorting in $\mathcal{O}(N \log N)$. In addition, the algorithm is parallelized and just-in-time compiled using Numba, providing significant acceleration.

For benchmarking, we compared our implementation to Jonathan Richard Shewchuk’s `Triangle` library²³, which provides a highly optimized Voronoi construction algorithm. This package is, to our knowledge, the fastest available implementation of two-dimensional Voronoi tessellation and therefore serves as a suitable baseline. We generated systems containing between 10^2 and 10^7 points, distributed uniformly at random in the unit square. For each system size, we prepared 128 independent realizations, and measured the average runtime and standard deviation. All calculations were performed on a machine running macOS 15.6 with an Apple M3 Max SoC and 64 GB of memory.

The benchmark results are shown in Fig. 12. For systems smaller than 1000 points, Voronoi outperforms both variants of SANN. For larger systems, however, the parallelized mSANN implementation consistently surpasses Voronoi, with speedups of up to $1.8\times$, while the sequential version remains the slowest across all system sizes. These results indicate that for small systems Voronoi remains the fastest option, but for simulations involving more than 10^3 points, parallelized mSANN offers the best computational speed.

III. CONCLUSION

We have revisited the SANN algorithm and examined its extension to two dimensions. While the defining relation of SANN is linear in three dimensions, it becomes nonlinear in two dimensions, leading to increased computational cost. Here, we examined the reformulated SANN introduced in Ref. 12 (SANNex) which approaches the cutoff determination as an existence–uniqueness problem, and avoids solving the nonlinear equation directly while retaining the efficiency and general features of the original method.

We also analyzed the tendency of both SANN and Voronoi to overcount neighbors in low-coordination-number lattices, an effect amplified in two dimensions. To mitigate this, we introduced the inscribed circle (sphere) modification, a parameter-free modification based on the relation between inscribed and circumscribed radii of regular polygons (polyhedra), which we called mSANN. We show that the correction yields more intuitive and robust results in both 2D and 3D.

Tests on ordered lattices showed that mSANN is more likely to identify a number of neighbors equal to the coordination number in open lattices, such as honeycomb, square, simple cubic, diamond, and graphite. In contrast, the original SANN remains mildly more robust in high-coordination environments such as hexagonal, FCC, and HCP lattices. Voronoi remained accurate in purely hexagonal regions but showed limitations elsewhere. In quasicrystalline tilings, mSANN typically directly yields the structure of the tiling, by avoiding the inclusion of diagonal bonds across squares seen in both Voronoi and SANN. For coexisting structures, mSANN provided consistent results across interfaces and defects.

Finally, performance benchmarks demonstrated that for small systems ($N < 10^3$) Voronoi remains faster, while for larger systems parallel mSANN consistently outperforms Voronoi by up to a factor of 1.8.

In summary, the proposed mSANN algorithm offers a parameter-free, computationally efficient, and robust approach to nearest-neighbor identification in two and three di-

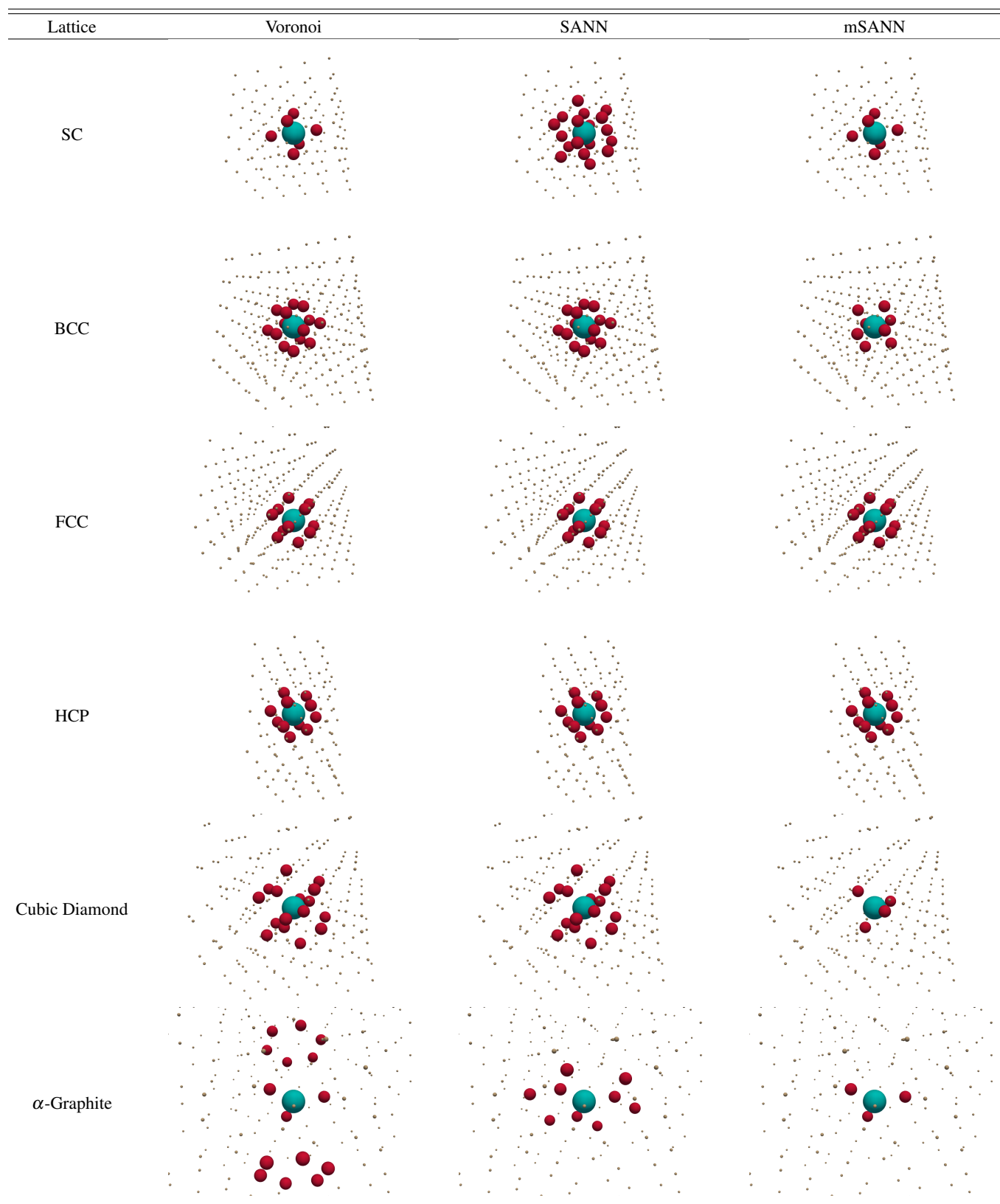


FIG. 7: Comparison of nearest-neighbor identification in ideal 3D lattices using Voronoi, SANN, and mSANN. Turquoise spheres indicate the central particle, crimson spheres its identified neighbors (scaled by 0.5), and tan spheres the remaining particles (scaled by 0.1).

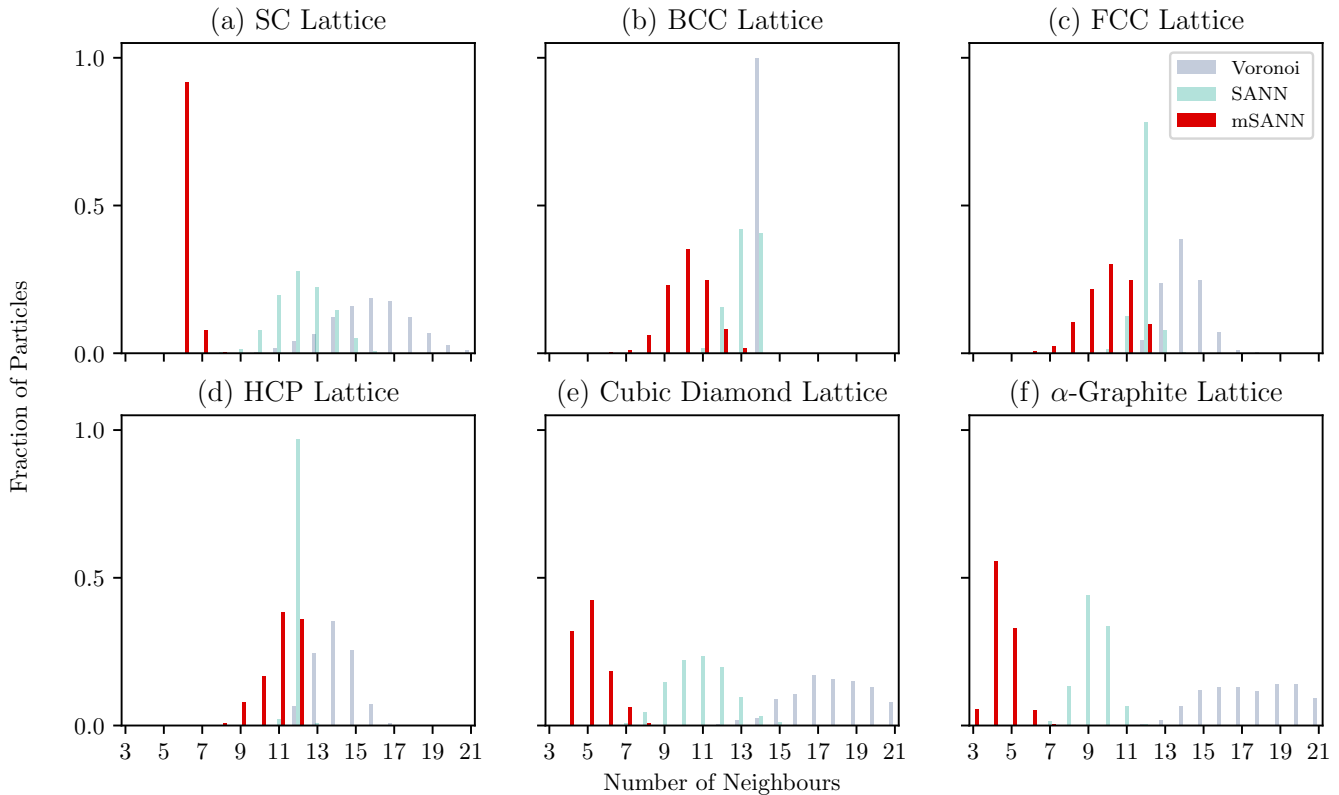


FIG. 8: Distributions of coordination numbers in 3D lattices identified using Voronoi, SANN, and mSANN. Systems correspond to those shown in Fig. 7.

mensions, that is particularly appropriate for systems with low coordination numbers, coexistence, and/or defects.

ACKNOWLEDGEMENTS

We would like to thank Geert H. A. Schulpen and Marjolein de Jager for fruitful discussions. A.U. and L.F. acknowledge funding from the XL research program with project number OCENW.GROOT.2019.071 which is financed by the Dutch Research Council (NWO).

DATA AVAILABILITY

All relevant data are available upon reasonable request.

- ¹P. J. Steinhardt, D. R. Nelson, and M. Ronchetti, “Bond-orientational order in liquids and glasses,” *Phys. Rev. B* **28**, 784 (1983).
- ²W. Lechner and C. Dellago, “Accurate determination of crystal structures based on averaged local bond order parameters,” *J. Chem. Phys.* **129**, 114707 (2008).
- ³A. Malins, S. R. Williams, J. Eggers, and C. P. Royall, “Identification of structure in condensed matter with the topological cluster classification,” *J. Chem. Phys.* **139**, 234506 (2013).
- ⁴W. F. Reinhart, A. W. Long, M. P. Howard, A. L. Ferguson, and A. Z. Panagiotopoulos, “Machine learning for autonomous crystal structure identification,” *Soft Matter* **13**, 4733–4745 (2017).

- ⁵E. Boattini, M. Dijkstra, and L. Filion, “Unsupervised learning for local structure detection in colloidal systems,” *J. Chem. Phys.* **151**, 154901 (2019).
- ⁶S. Fortune, “Voronoi diagrams and delaunay triangulations,” *Comput. Euclidean Geom.*, 225–265 (1995).
- ⁷J. Meijering, “Interface area, edge length, and number of vertices in crystal aggregates with random nucleation,” *Philips Res. Rep.* **8**, 270–290 (1953).
- ⁸W. Brostow, J.-P. Dussault, and B. L. Fox, “Construction of voronoi polyhedra,” *J. Comput. Phys.* **29**, 81–92 (1978).
- ⁹N. Medvedev, “The algorithm for three-dimensional voronoi polyhedra,” *J. Comput. Phys.* **67**, 223–229 (1986).
- ¹⁰J. A. van Meel, L. Filion, C. Valeriani, and D. Frenkel, “A parameter-free, solid-angle based, nearest-neighbor algorithm,” *J. Chem. Phys.* **136**, 234107 (2012).
- ¹¹M. Isobe, “Hard sphere simulation in statistical physics—methodologies and applications,” *Mol. Simul.* **42**, 1317–1329 (2016).
- ¹²D. Mugita, K. Souno, H. Koyama, T. Nakamura, and M. Isobe, “Simple and efficient methods for local structural analysis in polydisperse hard disk systems,” *J. Chem. Phys.* **160**, 174104 (2024).
- ¹³R. Staub and S. N. Steinmann, “Parameter-free coordination numbers for solutions and interfaces,” *J. Chem. Phys.* **152**, 024124 (2020).
- ¹⁴N. R. Varela-Rosales and M. Engel, “Solid-angle nearest-neighbor method for size-disperse systems of spheres,” arXiv preprint arXiv:2508.11220 (2025).
- ¹⁵D. Frenkel and B. Smit, *Understanding molecular simulation: from algorithms to applications* (Elsevier, 2023).
- ¹⁶P. Stampfli, “A dodecagonal quasicrystalline lattice in two dimensions,” *Helv. Phys. Acta* **59**, 1260 (1986).
- ¹⁷M. Oxborrow and C. L. Henley, “Random square-triangle tilings: A model for twelvefold-symmetric quasicrystals,” *Phys. Rev. B* **48**, 6966 (1993).
- ¹⁸T. Dotera, T. Oshiro, and P. Ziherl, “Mosaic two-lengthscale quasicrystals,” *Nature* **506**, 208–211 (2014).

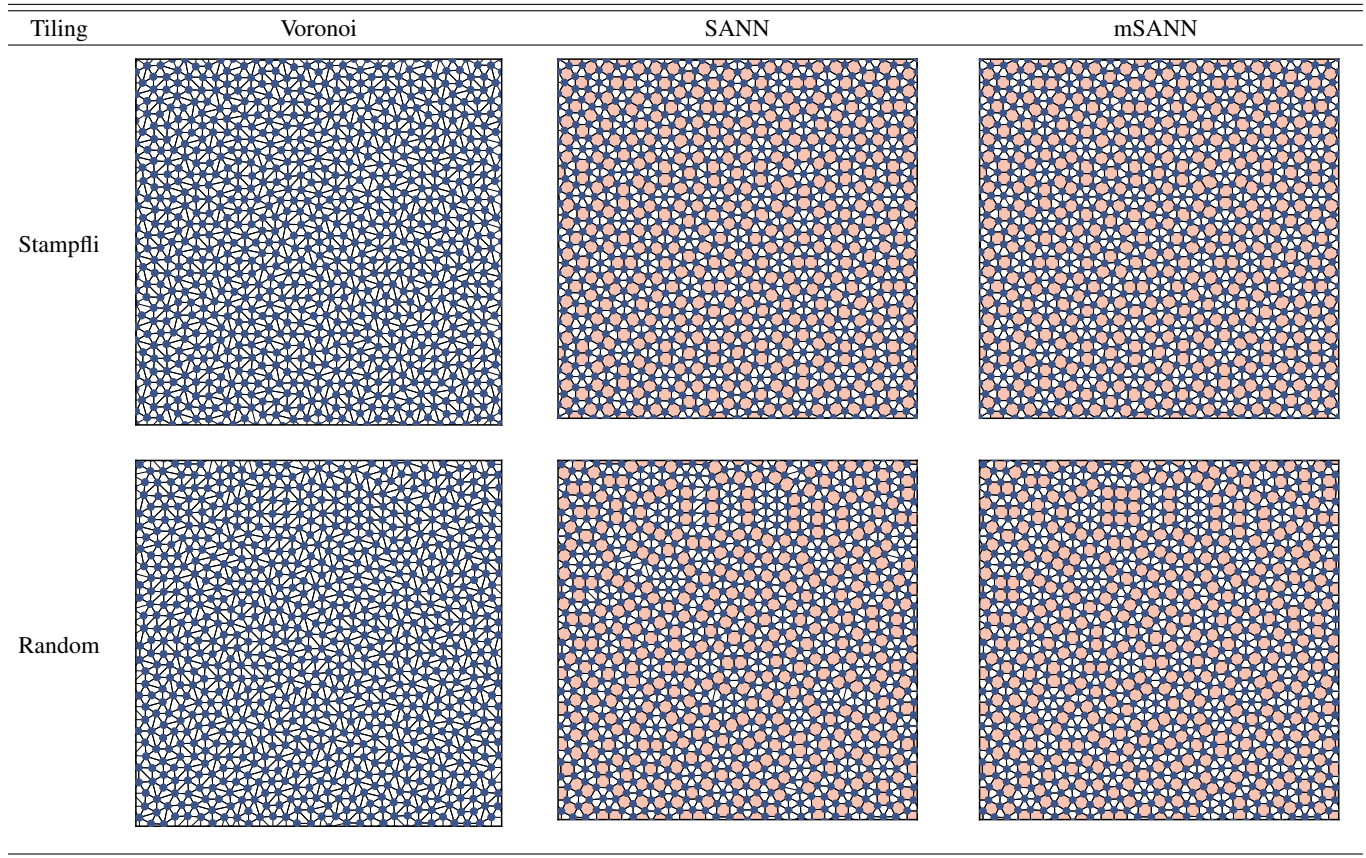


FIG. 9: Side-by-side comparison of nearest-neighbor identification using Voronoi construction, SANN and mSANN algorithms on 12-fold symmetric quasicrystal approximants. Dots represent particles and line segments connect identified neighbors. All lattices are simulated, thus, they include correlated thermal noise.

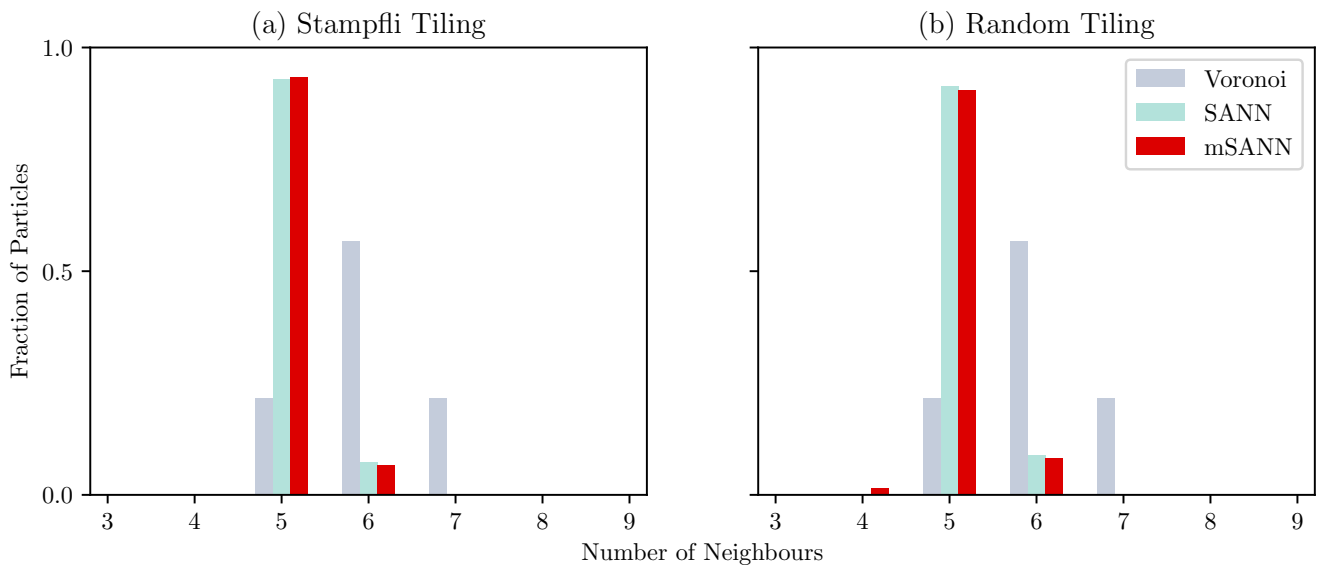


FIG. 10: The distributions of the number of nearest neighbors in a 12-fold symmetric (a) Stampfli-infilation , (b) random square-triangle tiling (depicted in Fig. 9) where nearest neighbors were identified by Voronoi construction, SANN, and mSANN.

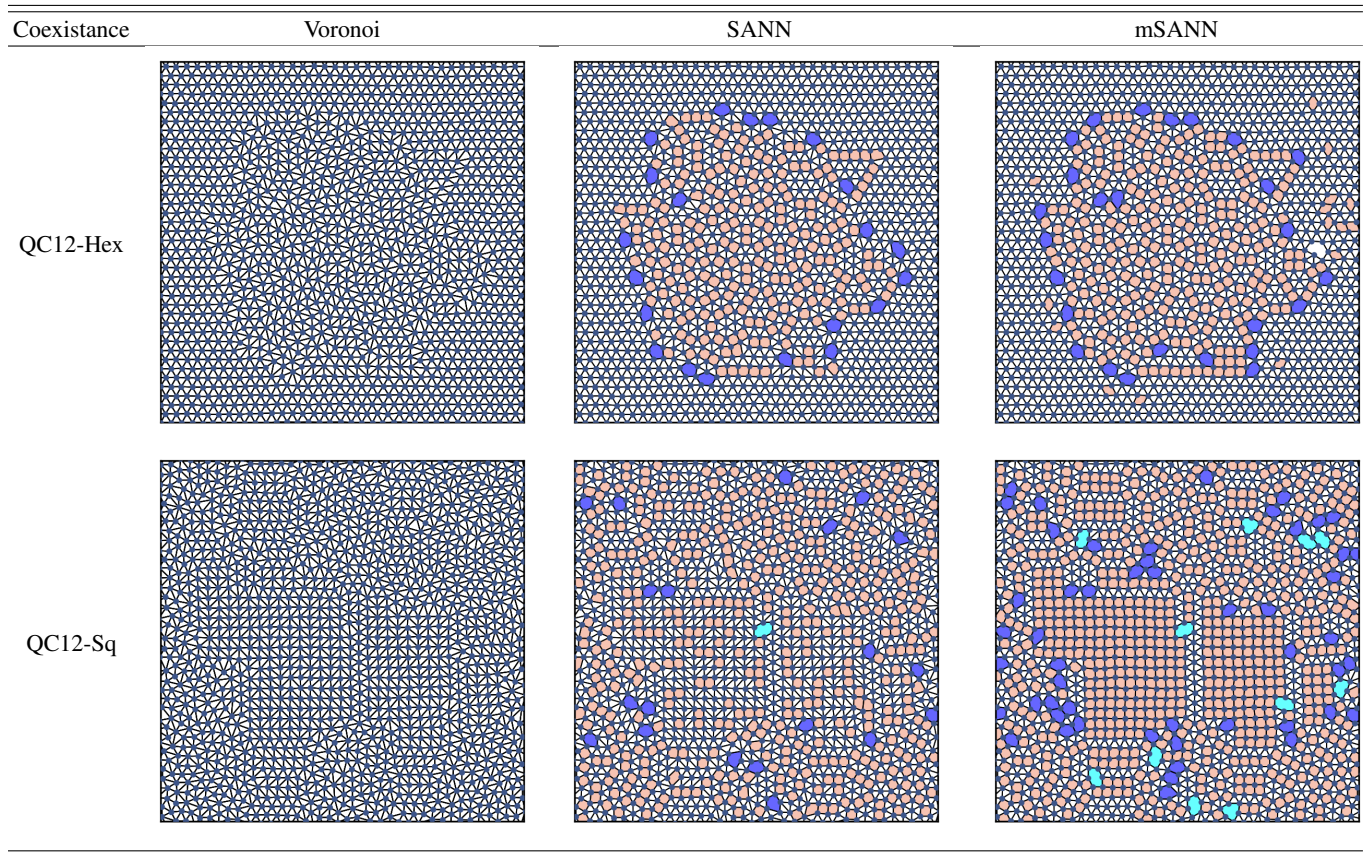


FIG. 11: Side-by-side comparison of nearest-neighbor identification using Voronoi construction, SANN and mSANN algorithms on 12-fold symmetric quasicrystal coexisting with the hexagonal and the square phases.

¹⁹H. Pattabhiraman, A. P. Gantapara, and M. Dijkstra, “On the stability of a quasicrystal and its crystalline approximant in a system of hard disks with a soft corona,” *J. Chem. Phys.* **143**, 164905 (2015).

²⁰H. Pattabhiraman and M. Dijkstra, “Phase behaviour of quasicrystal forming systems of core-corona particles,” *J. Chem. Phys.* **146**, 114901 (2017).

²¹F. Smallenburg, “Efficient event-driven simulations of hard spheres,” *Eur. Phys. J. E* **45**, 22 (2022).

²²A. Ulugö̇l, R. J. Hardeman, F. Smallenburg, and L. Filion, “Defects enhance stability in 12-fold symmetric soft-matter quasicrystals,” *Phys. Rev.*

Lett. **134**, 108201 (2025).

²³J. R. Shewchuk, “Triangle: Engineering a 2D Quality Mesh Generator and Delaunay Triangulator,” in *Applied Computational Geometry: Towards Geometric Engineering*, Lecture Notes in Computer Science, Vol. 1148, edited by M. C. Lin and D. Manocha (Springer-Verlag, 1996) pp. 203–222.

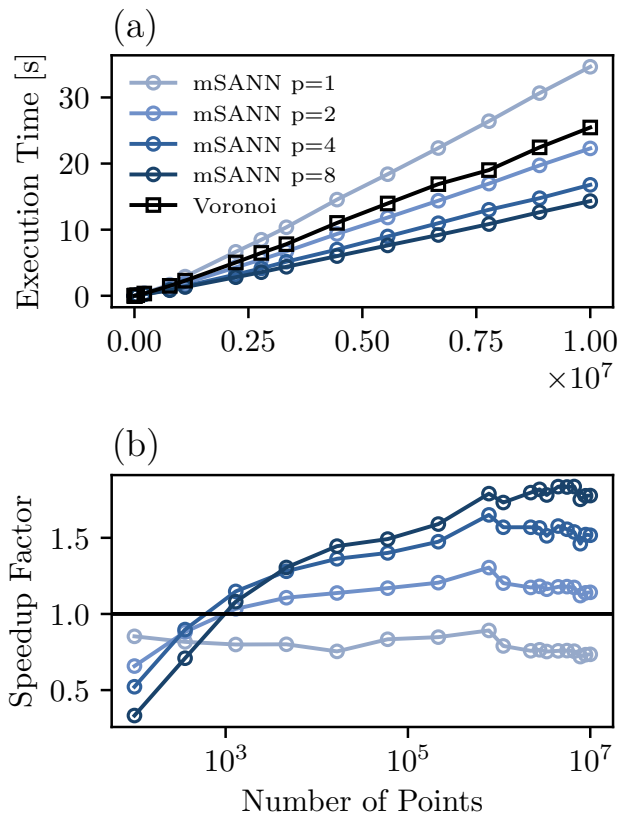


FIG. 12: Benchmark of our implementation of 2D mSANN versus Triangle's implementation of Voronoi construction. p is the number of cores used for the execution. Panel (a) shows the total execution time of the algorithms as a function of points in the configuration. Panel (b) shows the speedup factor, defined as ratio of the execution times of the Voronoi algorithm and the mSANN variants.